LANGMUIR APPLICATIONS LIST - [LP17]

LANGMUIR PROBE SYSTEM

The Impedans' Langmuir Probe system is used by academia and industry globally for plasma characterisation. Below is a list of publications with their plasma sources, process gases, pressures and applications.

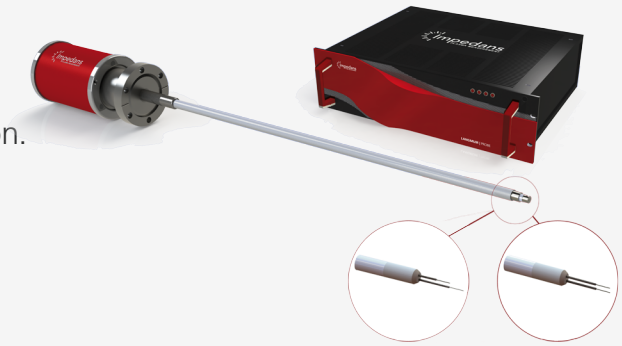

Plasma Source	Density (m^{-3})	Gas	Pressure(mTorr)	Published Paper
2.45 GHz MW	10^{14} -> 10^{17}	He,Ar,O_2,Air	10 -> 90	Characterization of a low-pressure microwave collisional-type coaxial plasma source used for decontamination in food industry
2.45 GHz Surface Wave	10^{11} -> 10^{15}	N_2 ,N_2,O_2	6000	Electrical characterization of the flowing afterglow of N2 and N2/O2 microwave plasmas at reduced pressure
2.45GHz ECR	10^{14} -> 10^{15}	Air	7.5	Investigation of bacterial spore inactivation using a 2.45 GHz coaxial plasma source
CCP	10^{14} -> 10^{15}	Ar, C	11.3	Suppression of a spontaneous dust density wave by a modulation of ion streaming
CCP	10^{15} -> 10^{16}	Ar	60 -> 400	Plasma parameters of RF capacitively coupled discharge comparative study between a plane cathode and a large hole dimensions multi-hollow cathode
CCP	10^{16}	-	<75	Analysis of double-probe characteristics in low-frequency gas discharges and its improvement
CCP	10^{15}	N_2	100 -> 1000	Capacitively coupled radio frequency nitrogen plasma generated at two different exciting frequencies of 13.56 MHz and 40 MHz analyzed using Langmuir probe along with optical emission spectroscopy
CCP	10^{16} -> 10^{17}	Ar	200 -> 500	Plasma parameters in 40 MHz Argon discharge
CCP	10^{15} -> 10^{16}	Ar, N_2	100 -> 1000	Synthesis and characterization of fluorene-type and hydrogenated amorphous carbon thin films in RF and DC glow discharges
CCP	10^{16} -> 10^{17}	Ar	525 -> 862	The Study of plasma parameters and the effect of experiment set up modification by using modelling software
CCP	10^{14} -> 10^{15}	Ar,H_2	75 -> 240	Comments on the Langmuir probe measurements of radio-frequency capacitive argon–hydrogen mixture discharge at low pressure
CCP	10^{15}	Ar	30 -> 500	An investigation of the spectral lines of argon discharge with Low electron density
CCP	10^{14}-> 10^{15}	Ar	50	Experimental and numerical investigations of the phase-shift effect in capacitively coupled discharges
CCP	10^{15} -> 10^{16}	H_2,Ar	112.5 -> 1725	Electrical Characteristics of Capacitive Coupled Radio Frequency Discharges in Argon and Hydrogen
CCP	10^{15}	Ar,H_2	585 -> 825	Optical and electrical properties of capacitive coupled radio frequency Ar-H2 mixture discharge at the low pressure
CCP	10^{14} -> 10^{15}	He	120 -> 180	Room temperature photoluminescence in plasma treated rutile TiO2 (110) single crystals
CCP	10^{16} -> 10^{18}	He	750	Density, temperature and magnetic field measurements in low density plasmas

Plasma Source	Density (m^{-3})	Gas	Pressure(mTorr)	Published Paper
CCP	10^{15} -> 10^{16}	He, Ar, O_2	225 -> 375	Evolution of plasma parameters in capacitively coupled He–O2/Ar mixture plasma generated at low pressure using 13.56 MHz generator
CCP	10^{17} -> 10^{18}	Ar	1500	In-Flight Size Focusing of Aerosols by a Low Temperature Plasma
CCP	10^{18}	Ga, Ar, N_2	4200	Nonequilibrium plasma aerotaxy of size controlled GaN nanocrystals
CCP	10^{14} -> 10^{15}	Ar, C	7.5	Observation of self-excited dust acoustic wave in dusty plasma with nanometer size dust grains
CCP	10^{16}	He, Air	915	The smooth effect of fast electron detection in the positive column in DC glow discharge
CCP	10^{16} -> 10^{17}	Ar	20	Control of ion energy distributions using phase shifting in multi-frequency capacitively coupled plasmas
CCP	10^{17} -> 10^{18}	Ar	1500 -> 10000	Low temperature plasma as a means to transform nanoparticle atomic structure
CCP	10^{15} -> 10^{16}	CO_2, H_2	1000	Langmuir Probe, optical and mass characterisation of a DC Co2-H2 plasma
CCP	NA	He	375	Evidence of effective local control of a plasma's nonlocal electron distribution function
CCP	0-> 200 A m^{-2}	Air	2 sccm	Design and characterisation of a plasma chamber for improved radial and axial film uniformity
CCP	10^{16} -> 10^{20}	Ar	1 atm	Characterisation of particle charging in low-temperature, atmospheric pressure, flow through plasmas
CCP	10^{14}-> 10^{16}	He/O_2	0.04->0.08 l/min	An investigation on optical properties of capacitively coupled radio-frequency mixture plasma with Langmuir probe
CCP (Plasmalab System 100)	0.1 -> 2 Am^{-2}	Ar	2	Ion energy distribution measurements in rf and pulsed dc plasma discharges
CCP/ICP	10^{15} -> 10^{17}	Ar	60 -> 600	Optical emission spectroscopy and collisional-radiative modeling for low temperature Ar plasmas
Dual CCP	10^{12} -> 10^{15}	N_2	100 -> 1000	Surface modification of unsized pan-based carbon fiber by using high frequency single and dual RF discharge system
Dual CCP	10^{17} -> 10^{19}	C_4F_8/Ar/O_2/N_2	30	Plasma induced damage reduction of ultra low-k dielectric by using source pulsed plasma etching for next BEOL interconnect manufacturing
Dual CCP	10^{13} -> 10^{15}	N_2	100 -> 700	Investigation of Single and Dual RF Capacitively Coupled Nitrogen Plasma Discharges Using Optical Emission Spectroscopy
Dual-Hybrid HiPIMS	10^{15} -> 10^{18}	Ar, Cu, Ti	2.25	Deposition of nanostructured Cu-Ti based films by advanced magnetron sputtering methods
Dual-Hybrid HiPIMS	10^{17} -> 10^{18}	Ar, Cu, Ti	3 -> 30	Time-resolved Langmuir probe investigation of hybrid high power impulse magnetron sputtering discharges
ECR	10^{14} -> 10^{16}	Ar,Air	3 -> 75	2.45 GHz ECR coaxial plasma source: characterization in single and multi-sources configuration
ECR	10^{16}	He, Ar	0.15 -> 0.9	Electric Potential build-up by trapped electrons in magnetically expanding plasma
Glow Discharge	10^{16} -> 10^{17}	He	112.5 -> 562.5	Properties of a large volume glow discharge helium plasma by measuring the broadband microwave phase shift in different pressures
Hall Thruster	10^{15} -> 10^{18}	Xe	13.5 -> 45	Anode geometry influence on LaB6 cathode discharge characteristics
Hall Thruster	10^{15} -> 10^{16}	Ar	30	Measurement of plasma parameters in the far-field plume of a Hall effect thruster
Hall Thruster	10^{16} -> 10^{17}	Xe	0.0015	Electron flow properties in the far-field plume of a Hall thruster
Hall Thruster	10^{15} -> 10^{16}	Xe, Kr	0.0225	Time-resolved measurement of plasma parameters in the far-field plume of a low-power Hall effect thruster
Hall Thruster	10^{16}	Xe	0.015	The time-varying electron energy distribution function in the plume of a Hall thruster

Plasma Source	Density (m^{-3})	Gas	Pressure(mTorr)	Published Paper
Hall Thruster	10^{16} -> 10^{18}	Xe	0.015	Electron energy distribution function in a low-power Hall thruster discharge and near-field plume
Helicon	10^{16} -> 10^{17}	Ar	2.6	Two density peaks in low magnetic field helicon plasma
Helicon	10^{15} -> 10^{16}	Ar	2.62	Modulation of absorption manner in helicon discharges by changing profile of low axial magnetic field*
Helicon	10^{16} -> 10^{18}	Ar	2.25	The Evolution of Discharge Mode Transition in Helicon Plasma Through ICCD Images
HiPIMS	10^{16} -> 10^{17}	Ar, Cr	0.5 -> 20	Spectroscopic investigation on the near-substrate plasma characteristics of chromium HiPIMS in low density discharge mode
HiPIMS	10^{13} -> 10^{17}	Ar, O_2, Ti	6.98	The behaviour of negative oxygen ions in the afterglow of a reactive HiPIMS discharge
HiPIMS	10^{16} -> 10^{18}	Ar, O_2, Ti	5.63	Design of magnetic field configuration for controlled discharge properties in highly ionized plasma
HiPIMS	10^{15} -> 10^{16}	Ar,O_2,Al	1.5	Investigating the plasma parameters and discharge asymmetry in dual magnetron reactive high power impulse magnetron sputtering discharge with Al in Ar/O2 mixture
HiPIMS	10^{16} -> 10^{17}	Ar,O_2,Ti	7.5	Angular dependence of plasma parameters and film properties during high power impulse magnetron sputtering for deposition of Ti and TiO2 layers
HiPIMS	10^{16} -> 10^{18}	Ar,O_2,Ti	5.63	Enhanced oxidation of TiO2 films prepared by high power impulse magnetron sputtering running in metallic mode
HiPIMS - ECWR	< 10^{18}	Ar, O_2, Ti	0.6 -> 75	Deposition of rutile (TiO2) with preferred orientation by assisted high power impulse magnetron sputtering
HiPIMS - ECWR	10^{16} -> 10^{18}	Ar, Ti	0.375	Plasma diagnostics of low pressure high power impulse magnetron sputtering assisted by electron cyclotron wave resonance plasma
HiPIMS (PLATTIT π)	10^{16} -> 10^{17}	Ar, Ti	4.9	Microstructure-driven strengthening of TiB2 coatings deposited by pulsed magnetron sputtering
Hot Cathode Plasma	10^{13}	Ar	0.8	Matched dipole probe for magnetized low electron density laboratory plasma diagnostics
Hot Cathode Plasma	10^{12} -> 10^{13}	Ar	0.15	Ion and electron sheath characteristics in a low density and low temperature plasma
Hollow Cathode	10^{15} -> 10^{18}	O_2	450 -> 825	Characterization and application of hollow cathode oxygen plasma
Hollow Cathode	10^{16}	Ar, Air	375 -> 750	Probe Diagnostics of Plasma Parameters in a Large-Volume Glow Discharge With Coaxial Gridded Hollow Electrodes
Hollow Cathode	10^{15} -> 10^{16}	Ar	187.5	Numerical and Experimental Diagnostics of Dusty Plasma in a Coaxial Gridded Hollow Cathode Discharge
Hollow Cathode	10^{16}	Ar	187.5	Investigation of Low-Pressure Glow Discharge in a Coaxial Gridded Hollow Cathode
Hollow Cathode	10^{16}	He	112.5	Diagnostics of large volume coaxial gridded hollow cathode DC discharge
Hollow Cathode	10^{16} -> 10^{17}	He	112.5 -> 562.5	Broadband microwave propagation in a novel large coaxial gridded hollow cathode helium plasma
Hollow Cathode	10^{15} -> 10^{16}	O_2	450 -> 787.5	Micro-grooving into thick CVD diamond films via hollow-cathode oxygen plasma etching
Hollow Cathode	10^{16}	Ar	112.5 -> 412.5	Broadband microwave characteristics of a novel coaxial gridded hollow cathode argon plasma
Hollow Cathode	10^{16}	Ar	150	Absolute continuum intensity diagnostics of a novel large coaxial gridded hollow cathode argon plasma
Hot Cathode Magnetic Filter	10^{11} -> 10^{12}	Ar, SF_6	0.165	Sheath characteristics in a magnetically filtered low density low temperature multicomponent plasma with negative ions
Hot Cathode Plasma	10^{13}	Ar	0.8	Matched dipole probe for magnetized low electron density laboratory plasma diagnostics

Plasma Source	Density (m^{-3})	Gas	Pressure(mTorr)	Published Paper
Hot Cathode Plasma	10^{12} -> 10^{13}	Ar	0.15	Ion and electron sheath characteristics in a low density and low temperature plasma
Hybrid – Dual- HiPIMS	10^{17} -> 10^{18}	Ar, Ti, Cu	3 -> 30	Time-resolved Langmuir probe investigation of hybrid high power impulse magnetron sputtering discharges
Hot filament Evaporator	10^{18}	Ar	6000	Phase mixing in GaSb nanocrystals synthesized by nonequilibrium plasma aerotaxy
CCP	10^{15} -> 10^{16}	Ar, Ar/O_2	150 -> 300	Temporal evolution of plasma parameters in a pulse-modulated capacitively coupled Ar/O2 mixture discharge
CVD	10^{16} -> 10^{17}	Ar	525 -> 900	The study of argon plasma based on experimental and modeling diagnosis
ICP	10^{16}	H_2	40	Numerical investigation of ion energy and angular distributions in a dc-biased H2 inductively coupled discharge
ICP	10^{16} -> 10^{17}	Ar, O_2	10 -> 50	Experimental and numerical investigations on time-resolved characteristics of pulsed inductively coupled O_2/Ar plasmas
ICP	10^{17}	H	3.75 -> 22.5	Investigation of the power transfer efficiency in a radio-frequency driven negative hydrogen ion source
ICP	10^{15}-> 10^{17}	H, Ar	2 -> 150	Investigation of a Magnetically Enhanced Inductively Coupled Negative Ion Plasma Source
ICP	10^{17} -> 10^{18}	Ar	3.75 -> 75	Nonlocal electron kinetics and spatial transport in radio-frequency two-chamber inductively coupled plasmas with argon discharges
ICP	10^{16} -> 10^{17}	Ar	10 -> 50	A hybrid model of radio frequency biased inductively coupled plasma discharges: description of model and experimental validation in argon
ICP	10^{17}	H	2.25	Development of RF Driver Used in Negative Ion Source at HUST
ICP	10^{16}	H	45	Study on the RF Power Necessary to Ignite Plasma for the ICP Test Facility at HUST
ICP	10^{15}	Ar	2 -> 10	Comparison of plasma parameters determined with a Langmuir probe and with a retarding field energy analyzer
ICP	10^{16} -> 10^{17}	H_2	2.25 -> 22.5	A global model study of the population dynamics of molecular hydrogen and the generation of negative hydrogen ions in low-pressure ICP discharge with an expansion region: effects of EEPF
ICP	10^{15}	Ar, H_2	40	Absolute density measurement of hydrogen atom in inductively coupled Ar/H2 plasmas using vacuum ultraviolet absorption spectroscopy
ICP	10^{16} -> 10^{17}	He	0.5 -> 2	Spatial distributions of plasma parameters in inductively coupled hydrogen discharges with an expansion region
ICP	10^{16} -> 10^{17}	H_2	0.75 -> 37.5	Experimental and numerical investigations of electron
ICP	N/a	CO_2, Ar, N_2	37.5 -> 1312	Tuning of Conversion and Optical Emission by Electron Temperature in Inductively Coupled CO2 Plasma
ICP	10^{16}-> 10^{17}	N_2	2.25	The discharge characteristics in nitrogen helicon plasma
ICP	10^{17}	CO_2, CO, O_2, Ar	5 -> 15	Study on plasma characteristics and gas analysis before and after recovery using liquid-fluorocarbon precursor
ICP	10^{17}	C_5F_8, C_5F_8/Ar	750	Superlocal chemical reaction equilibrium in low temperature plasma
Magnetic Mirror	10^{16}-> 10^{17}	N_2	0.2 -> 4	Signatures of ring currents in a magnetic mirror plasma experiment
Magnetron	10^{16}-> 10^{17}	Ar, Cu	0.75 -> 37.5	The erosion groove effects on RF planar magnetron sputtering
Magnetron	10^{16}-> 10^{17}	Ar	3000	Structural and plasma characterisation of the power effect on the chromium thin film deposited by DC magnetron sputtering
Magnetron	2 -> 70 Am^{-2}	Ar, N_2, Al	3.75	Tunable ion flux density and its impact on AlN thin films deposited in a confocal DC magnetron sputtering system
Magnetron	10^{16}-> 10^{17}	Ar, Ne Kr, Xe	5	Measurements of sputtered neutrals and ions and investigation of their roles on the plasma properties during rf magnetron sputtering of Zn and ZnO targets

Plasma Source	Density (m^{-3})	Gas	Pressure(mTorr)	Published Paper
MAGPIE	10^{17} -> 10^{19}	Ar, H_2	3.1	Design and characterization of the Magnetized Plasma Interaction Experiment (MAGPIE): a new source for plasma–material interaction studies
MAGPIE	10^{16}	H_2, N_2	10	A volume-averaged model of nitrogen–hydrogen plasma chemistry to investigate ammonia production in a plasma-surface-interaction device
MAGPIE	10^{18}	Ar	3	Wave modeling in a cylindrical non-uniform helicon discharge
MAGPIE	10^{16} -> 10^{17}	Ar	1.4 -> 3	Plasma parameters and electron energy distribution functions in a magnetically focused plasma.
MAGPIE	10^{16} -> 10^{17}	H	5 -> 10	Negative hydrogen ion production in a helicon plasma source
MAGPIE	< 10^{19}	H	10	Ion flux dependence of atomic hydrogen loss probabilities on tungsten and carbon surfaces
MW	10^{14}	Ar	150 -> 200	Apparatus for generating quasi-free-space microwave-driven plasmas
MW	10^{15} -> 10^{16}	He	525	Microwave technology used for plasma diagnostic in complicated situations
MW	10^{16} -> 10^{17}	Ar, O_2	75 -> 225	Heating power at the substrate, electron temperature, and electron density in 2.45 GHz low-pressure microwave plasma
MW	10^{17} -> 10^{18}	He, Ar	1000 -> 10000	A prospective microwave plasma source for in situ spaceflight applications
NExET	10^{18}	Xe	15	Anode position influence on discharge modes of a LaB6 cathode in diode configuration
NExET	10^{15} -> 10^{18}	Xe	13.5 -> 45	Anode geometry influence on LaB6 cathode discharge characteristics
NExET	10^{17} -> 10^{18}	Xe	0.8 mg s^{-1}	Electron properties of an emissive cathode: Analysis with incoherent thomson scattering, fluid simulations and Langmuir probe measurements
PEGASES Thruster	10^{15} -> 10^{17}	Ar, Xe	0.75	Investigation of Magnetized radio frequency plasma courses for electric space propulsion
PEGASES Thruster	10^{18}	SF_6, Ar, Xe, He, O_2, N_2	0.75	Plasma drift in a low-pressure magnetized radio frequency discharge
PPS 1350-ML Hall Thruster	10^{16} -> 10^{17}	Xe	0.0015	Electron flow properties in the far-field plume of a Hall thruster
PPS100-ML Hall Thruster	10^{15} -> 10^{16}	Xe	2.92 -> 4.5 mg s^{-1}	Measurement of plasma parameters in the far-field plume of a Hall effect thruster
Pulsed ICP	10^{15} -> 10^{16}	CH_4,O_2,Ar	0.975	Nanometer-scale etching of CoFeB thin films using pulse-modulated high density plasma
Pulsed ICP	10^{16} -> 10^{17}	Ar, CF_4	1 -> 80	Complex transients of input power and electron density in pulsed inductively coupled discharges
Pulsed Laser Deposition	10^{16}	O_2, WO_3	7.5	Optimization of substrate-target distance for pulsed laser deposition of tungsten oxide thin films using Langmuir probe
Pulsed Laser Deposition	10^{16} -> 10^{17}	O_2, CeO_2	7.5	Plasma plume behavior of laser ablated cerium oxide: Effect of oxygen partial pressure
Proton Linear Accelerator	10^{18} -> 10^{19}	H	1.125 -> 5	Plasma characterization of the superconducting proton linear accelerator plasma generator using a 2 MHz compensated Langmuir probe
PULVA reactor	10^{15}	Ar, C_2H_2	15 -> 30	Metastable argon atom density in complex argon/acetylene plasmas determined by means of optical absorption and emission spectroscopy
VHF Multi-tile Push-Pull	10^{16} -> 10^{17}	N_2	5 -> 25	Nitriding process for next-generation semiconductor devices by VHF (162 MHz) multi-tile push-pull plasma source

*Click here to read more about Langmuir Probe System.

*Click here to download the Langmuir Probe System brochure.

Impedans Ltd
Chase House
City Junction Business Park, Northern Cross
Dublin - D17 AK63, Ireland

Tel: +353 1 842 8826
Email: sales@impedans.com
www.impedans.com